Effects of Water Injection on Generator Output Power Augmentation in a Microturbine

Kojun Suzuki, Susumu Nakano, Keiichi Seki, Yoichi Takeda, Tadaharu Kishibe

Effects of Water Injection on Generator Output Power Augmentation in a Microturbine

Kojun Suzuki[1]*, Susumu Nakano[1]*, Keiichi Seki[1]*, Yoichi Takeda[1]*, Tadaharu Kishibe[2]*

ISROMAC 2017

International Symposium on Transport Phenomena and Dynamics of Rotating Machinery

Hawaii, Maui
December 16-21, 2017

Abstract

Both water atomizing inlet air cooling (WAC) and the evaporative gas turbine cycle are methods to improve gas turbine efficiency and output using water evaporation. Especially, small-amount water injection methods which are used in WAC and the recuperative water injected (RWI) cycle are relatively easy to implement in existing turbines, and they are effective ways to increase output power for microturbines. The purposes of this study are to develop a dynamic simulator which can handle WAC and RWI operations and to clarify the quantitative contribution to power augmentation by the effect of water injection. Heat penetration from the turbine to the compressor which affects the performance of the turbine system is considered in the simulator. Simulation results are compared with measured results which were previously obtained in the operation test of the 150 kW class prototype microturbine. Good agreement is seen between the simulation and measured results for the main output data such as the compressor discharge pressure and the generator output power. In the total output power augmentation of the generator by WAC and RWI operations, about 1/3 is brought about by the reduction of the compressor driving power and about 2/3 is brought about by the increase of the turbine output power. Simulation results also show a big effect from the heat penetration to the compressor on the generator output power.

Keywords

Microturbine — Dynamic simulation — Evaporative gas turbine cycle — Water Injection

[1] *Department of Mechanical Engineering, Tohoku University, Sendai, Japan*

[2] *Mitsubishi Hitachi Power Systems, Ltd., Hitachi, Japan*

*__Corresponding author__: susumu.nakano@rift.mech.tohoku.ac.jp

INTRODUCTION

Microturbines, which were launched into the power market at the end of the 1990's, are still in a difficult situation with respect to their spread in the market because of their low electric efficiencies. Though microturbines have high efficiency in small-scale combined heat and power (CHP) systems [1], this good feature is still limited to their heat-driven use.

To raise their electric efficiency, water atomizing inlet air cooling (WAC), which has already been applied in large-scale gas turbines, and a humid air turbine (HAT) cycle, which was demonstrated in a small-capacity gas turbine [2], have been tried for microturbines. Williamson et al. [3] demonstrated the validity of WAC by applying an evaporation cooling system to a commercial microturbine. In the early stage of microturbine development, Parente et al. [4] analyzed the effectiveness of the HAT application to microturbines which applied a saturation tower to increase humidity. The first actual application test of the spray saturation tower to a commercial microturbine was conducted by De Paepe et al. [5], and operation characteristics including those for partial load were shown. Nakano et al. [6] made the first application of an evaporative gas turbine cycle to a microturbine with a 150 kW class prototype machine. Nakano et al. also applied WAC, and found that even when quite a small amount of water was supplied by spray nozzles, the effectiveness of power augmentation of the microturbine and the quick response to power rise were shown. However, the quantitative contribution to generator output power augmentation by injected water has not been made entirely clear. How much of the augmentation of the generation power was derived from the increase of turbine power output or from the reduction of the compressor driving power has remained unknown.

It is difficult to analyze the quantitative contribution to power augmentation by the effect of injected water using only the data of a prototype machine operation test because the measured generator output power includes both effects of the turbine power increase and the compressor power reduction. A dynamic simulator is expected to be a useful tool to understand dynamic characteristics of the turbine system because each effect of individual system components can be separated in the calculation result.

The purposes of this study are to develop a dynamic simulator which can handle WAC and recuperative water injected (RWI) cycle operations and to clarify the quantitative contribution to power augmentation by the effect of water injection. This simulator is an in-house code written in FORTRAN. Simulation results are compared with measured data which were obtained in the operation test of the 150 kW class prototype microturbine [6]. As the compressor impeller and the turbine wheel are located very close to each other in the microturbine, heat penetration from the turbine to the compressor influences the effect on the performance of the turbine system because the compressor driving

power increases due to the heat penetration. A simple heat transfer model is considered in the simulator to check the effect of the heat penetration.

NOMENCLATURE

A	Cross-sectional area of duct [m^2]
C	Convectional heat transfer [W/m^2]
C_p	Specific heat with constant pressure [J/(kg K)]
D	Diameter [m]
D_f	Diffusivity [m^2/s]
G	Flow rate [kg/s]
H	Enthalpy [J]
H_u	Low heat value of fuel [J/kg]
I	Inertia moment [kg m^2]
L	Latent heat of water droplet [J/kg]
L_e	Specific Euler work [J/kg]
N	Rotational speed [rpm]
N_d	Number of water droplets
N_u	Nusselt number
P	Pressure [Pa]
P_r	Prandtl number
Q	Heat transfer with water droplet evaporation [W]
R	Radiation heat transfer [W/m^2]
R_e	Reynolds number
S	Surface area [m^2]
S_c	Schmidt number
S_h	Sherwood number
T	Temperature [K]
V	Inlet or outlet velocity of compressor [m/s]
W	Power or output [W]
W_{loss}	Windage loss, bearing loss [W]
Y	Mass fraction of vapor
f	Exponential function, polynomial function and cubic function
h	Specific enthalpy [J/kg]
m	Mass of a water droplet or mass of air surrounding a water droplet [kg]
t	Time [s]
u	Circumferential velocity [m/s]
x	Wetness of wet air
$x_{ev,RWI}$	Wetness added by RWI
ΔQ	Heat transfer into or from compressor [W/kg]
β	Ratio of the meridional direction component of absolute velocity to circumferential velocity at average radius of compressor inlet
η	Efficiency
κ	Specific heat ratio
η_B	Combustion efficiency
η_{PTO}	Polytrophic efficiency
η_{rec}	Recuperator effectiveness
λ	Thermal conductivity [W/(m K)]
ξ_C	Friction coefficient
ρ	Density [kg/m^3]
ω	Angular velocity [rad/s]

Subscripts

C	Compressor
G	Generator
T	Turbine
a	Dry air
atm	Atmosphere
cmb	Combustor
cir	Circumferential direction
cr	Corrected value
csng	Casing
d	Water droplet
dsgn	Designed value
ev	Evaporation
f	Fuel
g	Combustion gas
in	Inlet
jb	Journal bearing
liner	Combustor liner
mean	Mean diameter
out	Outlet
rec	Recuperator
ref	Referential value
rs	Rated rotation
tb	Thrust bearing
wa	Wet air
0	Total
1	From combustion gas to liner
2	From liner to cooling air
3	From cooling air to casing

1. OVERVIEW OF THE MICROTURBINE APPLYING WAC AND RWI

The thermodynamic cycle applied to microturbines is generally the regenerative Brayton cycle. Figure 1 shows the system diagram of the one referred to in this study. The prototype machine was not a commercial one but one developed as an application machine of the evaporative gas turbine cycle [6]. The main components are a single-stage centrifugal compressor, a single-stage radial turbine, a can type combustor, a recuperator, a permanent magnet generator, and an electrical conversion system. The main feature of this microturbine system is utilization of water for improved electrical output and lubrication of bearings [7]. Application of water lubricated bearings reduces bearing loss. Water is also used for the cooling system of the generator and the electrical conversion system. There are two water supply lines that include the WAC and RWI lines and a water circulation line for the electrical equipment cooling. Water for WAC and RWI is purified with a reverse osmosis membrane.

The arrangement of the main components of the prototype microturbine is shown in Fig. 2. Atmospheric air is taken in and compressed by the centrifugal compressor. Compressor discharged air is sent to the recuperator and warmed up by heat exchange of the turbine exhaust gas. Compressed and heated-up air is sent to the combustor through the outer flow path of the turbine casing and the flow path between the combustor liner (hereafter, simply designated as liner) and the combustor casing. The combustion gas drives the turbine rotor and is exhausted through the recuperator to the atmosphere. Water spray for WAC is provided in the inlet duct of the compressor and that for RWI is provided in the straight duct set between the

compressor and the recuperator. Design specifications of the microturbine are given in Table 1. The design specifications are at the air temperature of 15 °C and atmospheric pressure of 101.3 kPa. The impellor of the centrifugal compressor and the turbine rotor were designed to be suitable for use both with and without RWI and WAC operations because the maximum mass flow rate of supplied water for WAC and RWI is limited to only 2 - 3 % of the inlet air mass flow rate of the compressor.

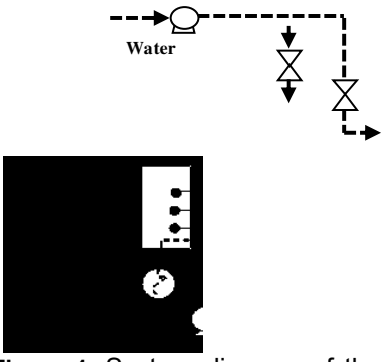

Figure 1. System diagram of the objective microturbine system [6]

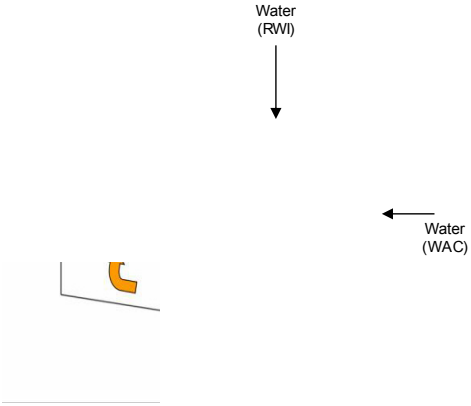

Figure 2. Perspective view showing arrangement of the main components of the microturbine [6]; colored arrows show the flow of working fluid

Table 1. Design specifications of the prototype microturbine [6]

Specification		Unit	Design
Rated output	without WAC and RWI	kW	129
	with WAC and RWI	kW	150
Efficiency(LHV)	without WAC and RWI	%	32.5
	with WAC and RWI	%	35
Rated rotational speed		rpm	51,000
Pressure ratio of compressor		-	4
Turbine inlet temperature		℃	960
Rated recuperator effectiveness		-	92
Bearing lubricant		-	water

2. SIMULATION MODELS

Dynamic behavior of the turbine system can be obtained to calculate time integration of an angular momentum equation of the rotor. The state changes of each component of the turbine system in an infinitesimal time are assumed to be quasi-steady-state [8] [9], and they are calculated from mass and enthalpy balances between an inlet and outlet of each component which is considered as a volume-less component [10]. Simulation models of the components and other quantities relating to them are described next.

2.1 Momentum Equation of Rotor

The motion of the turbine rotor is expressed by a conservation equation of angular momentum. Time change of the square of the angular velocity can be written as the summation of all types of work acting on the rotor.

$$\frac{d\omega^2}{dt} = \frac{2}{\mathrm{I}}(W_T - W_C - W_{loss} - W_G) \tag{1}$$

2.2 Centrifugal Compressor

2.2.1 Mass flow rate of air and pressure ratio

Mass flow rate of air that flows into the compressor is expressed in Eq. (2) using the relationship between the velocity triangle and the meridional direction component of the absolute velocity of the compressor inlet.

$$G_{wa} = \mathrm{A}_{\mathrm{C,in}}\rho_{wa,C,in}\beta\frac{\mathrm{D}_{\mathrm{C,mean}}}{2}\omega \tag{2}$$

Here β is the ratio of the meridional direction component of absolute velocity to circumferential velocity at the average radius of the compressor inlet. As β is a variable which varies with operation conditions, β is adjusted to fit a running curve on a performance characteristic map of the compressor. Figure 3 shows the characteristic map of the compressor and the running curve. Below the region of the rated rotational speed, inlet velocity coefficient β is assumed to be a function of only the rotational speed because operation is at almost no load. β is given as an exponential function f_ω of the rotational speed. After reaching the rated rotational speed, β is defined by a quadratic function f_W of the generator output power and it is expressed by Eq. (3).

$$\beta = f_\omega(\omega), \quad \beta_{\omega=\omega_{rs}} = f_W(W_G) \tag{3}$$

Relationships between pressure ratios and mass flow rates are drawn for each rotational speed in the running curve. Corrected mass flow rate and corrected rotational speed which are given in Eq. (4) are usually used.

$$G_{cr} = G\frac{p_{ref}}{p}\sqrt{\frac{T}{\mathrm{T}_{\mathrm{ref}}}}, \quad N_{cr} = N\sqrt{\frac{\mathrm{T}_{\mathrm{ref}}}{T}} \tag{4}$$

In the map of the characteristic curves of the compressor, pressure ratios are expressed by the corrected mass flow rate and the corrected rotational speed. Those characteristic curves can be expressed by cubic functions f_n of the corrected mass flow rate for each corrected rotational speed as given in Eq. (5).

$$\left(\frac{p}{p_{atm}}\right)_{\omega_n} = f_n\left(G_{cr,\omega_n}\right) \tag{5}$$

Pressure ratio at any rotational speed can be calculated as the interpolated equation for the rotational speed between the two characteristic lines. A similar method is applied to calculations of compressor efficiencies for each operation condition.

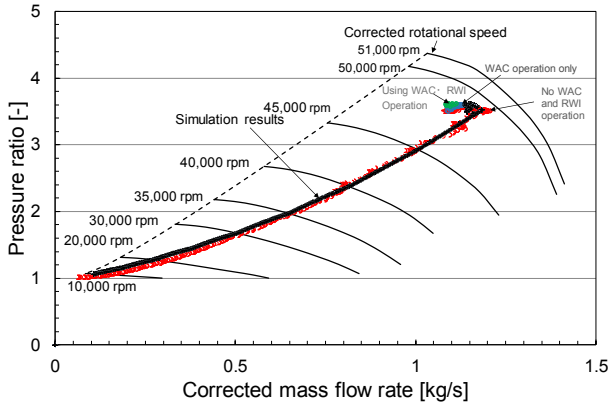

Figure 3. Characteristic map and running curve of compressor

2.2.2 Driving power

The driving power of the centrifugal compressor *Wc* is calculated in Eq. (6) with the Euler work of air done by the centrifugal compressor, friction loss of the compressor impeller which is assumed to be in proportion to the kinetic energy of air at the outlet of the compressor, and the heat transfer into or from the compressor. The friction loss coefficient ξ_c that is applied is for a rotating disk [11].

$$W_c = \frac{1}{\eta_c}(1+x)G_a\left(L_e + \xi_c \frac{u_{c,out}^{\ 2}}{2} + \Delta Q\right) \tag{6}$$

$$L_e = V_{out,cir}u_{out} - V_{in,cir}u_{in,mean} \tag{7}$$

There are two kinds of heat transfer. One is heat penetration from the turbine wheel which is set in a back-to-back configuration for the compressor impeller divided by the barrier wall. The other is the latent heat of the water droplet evaporation in the compressor which takes the heat from the working fluid of the compressor when WAC is operated. It is called wet compression [12]. The effect of the wet compression on the characteristic map of the compressor is neglected because the flow rate of WAC is about 0.5 % of the air flow rate which is shown in Section 3.2.

2.3 Combustor

Gas temperature at the combustor outlet is calculated from the enthalpy of combustion gas for the unit fuel flow rate and enthalpy of cooling air for the unit air flow rate which are expressed in Eqs. (8) and (9) with heat losses. Radiation heat transfer R and convection heat transfer C are considered as heat losses [13]. These heat transfer values for the present study reach about 8 kW for radiation (R_1S_{liner}) and about 2 kW for convection (C_1S_{liner}) around the rated rotational speed condition. As the fuel is natural gas, the flue gas is composed of N_2, O_2, CO_2, and H_2O because the combustion is assumed to be complete combustion. Combustion efficiency η_B reaches almost 1 at the steady state of the rated rotational condition. However, it is difficult to define combustion efficiency during warming-up of the recuperator. As the combustion efficiency was measured in the prototype operation test [6], the measured result of η_B is used in the simulations.

$$h_{g,cmb,out} = h_{wa,C,out}\frac{A_{liner}}{A_{cmb}}G_{wa} + h_f G_f + \eta_B H_u G_f - \frac{(R_1+C_1)S_{liner}}{G_f} \tag{8}$$

$$h_{wa,cmb,out} = h_{wa,C,out} + \frac{C_2 S_{liner} - C_3 S_{csng}}{\frac{A_{cmb}-A_{liner}}{A_{cmb}}G_{wa}} \tag{9}$$

2.4 Radial Inflow Turbine

Gas temperature of the turbine inlet is obtained from that of the combustion gas taking into consideration heat loss in the volute of the turbine. Temperature of the turbine inlet, is calculated from the temperature of combustion gas and cooling air. A tentative gas temperature of the turbine outlet is calculated with the assumption of the adiabatic change for the calculation of the turbine output power. Output power of the turbine is calculated using the adiabatic efficiency of the turbine and enthalpy difference between the turbine inlet and outlet.

$$W_T = \eta_T G_f\left(h_{0,T,in} - h_{0,T,out}\right) \tag{10}$$

Here, adiabatic efficiency of the radial inflow turbine η_T is calculated using model equations [14] which are formed from existing published data [15]. After the turbine power calculation, gas temperature of the turbine outlet is recalculated using polytrophic efficiency.

$$T_{T,out} = T_{T,in}\left(\frac{P_{T,out}}{P_{T,in}}\right)^{\eta_{PTO}\frac{\kappa-1}{\kappa}} \tag{11}$$

Polytrophic efficiency is determined by using the pressure ratio and the adiabatic efficiency of the turbine shown in Eq. (12).

$$\eta_{PTO} = \frac{\log\left[1-\eta_T\left(1-\left(\frac{P_{T,out}}{P_{T,in}}\right)^{\frac{\kappa-1}{\kappa}}\right)\right]}{\log\left(\frac{P_{T,out}}{P_{T,in}}\right)^{\frac{\kappa-1}{\kappa}}} \tag{12}$$

2.5 Recuperator

Temperature of air pressurized by the compressor is raised through heat exchange in the recuperator. The temperature is calculated in Eq. (13) with recuperator effectiveness.

$$T_{cmb,in} = T_{rec,in} + \eta_{rec}\left(T_{T,out} - T_{rec,in}\right) \tag{13}$$

The recuperator effectiveness is strongly affected by the structure of the recuperator, temperature and flow rate of air passed through the recuperator. Though it is preferable for the simulation model of the recuperator to consider these items, some important data such as the overall coefficient of heat transfer and surface area of heat transfer have not been disclosed as they are the manufacturers' proprietary information. Therefore, a simple model is applied; this model is assumed to satisfy the design conditions of the recuperator effectiveness for temperature and flow rate of air when the rotational speed reaches the rated rotational speed. The recuperator effectiveness is given as the product of its design value and the ratio of the rotational speed to the rated rotational speed. This is shown in Eq. (14).

$$\eta_{rec} = \frac{T_{cmb,in} - T_{rec,in}}{T_{T,out} - T_{rec,in}} = \eta_{\mathrm{rec,dsgn}} \frac{\omega}{\omega_{\mathrm{rs}}} \tag{14}$$

2.6 Windage and Bearing Losses

Total loss of the rotor is given in Eq. (15). Windages of the compressor and turbine are approximated as windages of rotating disks [16]. Journal and thrust bearing losses from prototype operation tests for the bearing [7] are applied.

$$W_{loss} = W_{loss,c} + W_{loss,T} + W_{loss,r} + W_{loss,jb} + W_{loss,tb} \tag{15}$$

2.7 WAC and RWI

A single droplet evaporation model [17] is used as the simulation model for WAC and RWI. Injection water consists of a number of droplets. The initial diameter of a droplet is given as input data. The number of droplets is calculated by the flow rate of injected water. Each droplet has a wet air region surrounding it. The heat and mass are exchanged between the droplet and the wet air. The temperature changes of the droplet and wet air are given by Eqs. (16) and (17).

$$\frac{dT_d}{dt} = \frac{Q - \frac{dm_{d,ev}}{dt}\mathrm{L}}{m_d C_{p,d}} \tag{16}$$

$$\frac{dT_a}{dt} = \frac{-Q}{m_{wa} C_{p,wa}} \tag{17}$$

Here, the amount of heat transfer Q is expressed by Eq. (18) and Nusselt number N_u is given in Eq. (19).

$$Q = \pi D_d \lambda (T_{wa} - T_d) N_u \tag{18}$$

$$N_u = 2 + 0.552 R_e^{1/2} P_r^{1/3} \tag{19}$$

The amount of the mass transferred from the droplet to the wet air is given by Eqs. (20) and (21), assuming the analogy between heat and mass transfers [18]

$$m_{d,ev} = \pi D_d \rho D_f (Y_d - Y_{wa}) S_h \tag{20}$$

$$S_h = 2 + 0.552 R_e^{1/2} S_c^{1/3} \tag{21}$$

where S_c is Schmidt number and S_h is Sherwood number. For a reference temperature in the calculation, such as for heat conductivity and diffusivity, the 1/3 rule is applied [19].

Residual droplets, which cannot be evaporated completely in the inlet region of the compressor, enter the flow path between the impellers of the compressor and they continue to evaporate as they move through the passage of the impellers. This causes a wet compression effect. The wet compression effect is considered in this simulator. Residual droplets which cannot be evaporated completely in the passage of the rotating impellers are assumed to evaporate completely in the volute region of the compressor outlet. Enthalpy possessed in the residual droplets is added to the wet air enthalpy at the outlet of the compressor. RWI is implemented at the straight duct set in the upstream region of the recuperator. Similar calculations as for the WAC are applied for RWI. Both the temperature decrease of wet air and the mass increase of wet air occur at the inlet of the recuperator. Enthalpy at the inlet of the recuperator $H_{rec,in}$ is expressed in Eq. (22).

$$H_{rec,in} = G_a h_a + G_a (x + x_{ev,RWI}) h_{wa} + N_d \left[(m_d - m_{d,ev}) h_d + m_{d,ev} L \right] \tag{22}$$

3. MEASURED RESULTS AND SIMULATION CONDITIONS

3.1 Measured results

Temperatures and pressures at the major points of the prototype microturbine were measured in the prototype operation test [6]. Inlet air flow rate of the compressor was measured by using the difference pressure of the air filter which was set in the inlet duct of the compressor. Fuel flow rate and injection water were each measured with a gas flow meter (model no. TF-2441; Tokyo Instrumentation) and a water mass flow meter (model no. FD-M; Keyence). These instruments have the maximum measurement errors of ±4.6 % for the water mass flow meter and ±0.2 % for the gas flow meter.

The generator output power, which is expressed by W_G in Eq. (1), was given by the generator output on the generator end measured with a power meter (model no. WT1600; Yokogawa) divided by the generator efficiency. The maximum measurement error of the power meter is ±0.15 %. The generator efficiency was calculated using the generator loss which was estimated from the flow rate of the cooling water and temperature rise of the cooling water between the outlet and inlet of the generator stator [20].

The compressor driving power was calculated using the measured total temperature at the inlet and outlet of the compressor as shown in Eq. (23). The turbine output power was also calculated by the measured value of the total temperatures at the inlet and the outlet of the turbine as shown in Eq. (24). Mass flow rate of the turbine passage was the summation of measured air flow rate of the compressor and the measured fuel flow

rate.

$$W_C = G_{wa,c}\left(C_{p,c,out}T_{0,c,out} - C_{p,c,in}T_{0,c,in}\right) \quad (23)$$

$$W_T = G_{g,T}\left(C_{p,T,in}T_{0,T,in} - C_{p,T,out}T_{0,T,out}\right) \quad (24)$$

3.2 Simulation Conditions

There were two groups of input data. One group included the turbine specifications data such as representative sizes of the impellers of the compressor, the turbine rotor, the combustor, and the inertia moment of the rotor, and so on. The other group included operation data of the rotational speed, fuel flow rate, and injection water flow rates for WAC and RWI [6]. Input data of the rotational speed and fuel flow rate are shown in Fig. 4, and injection water flow rates of WAC and RWI are shown in Fig. 5.

As the prototype microturbine operation test for RWI was the first application of RWI to a microturbine, the maximum rotational speed was controlled at 50,490 rpm, which was below the design rated speed of 51,000 rpm to keep a safe operation condition for controlling the machine if a sudden increase of the generator output power occurred when water supply to the system was started. Actually, after 3,200 s had passed, the rotational speed was further decreased to 49,990 rpm.

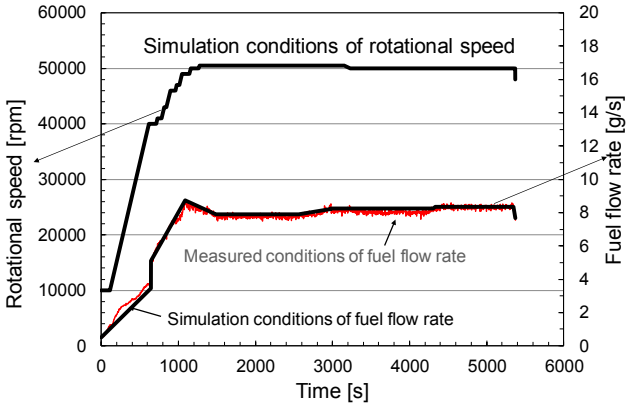

Figure 4. Simulation conditions of rotational speed fuel flow rate

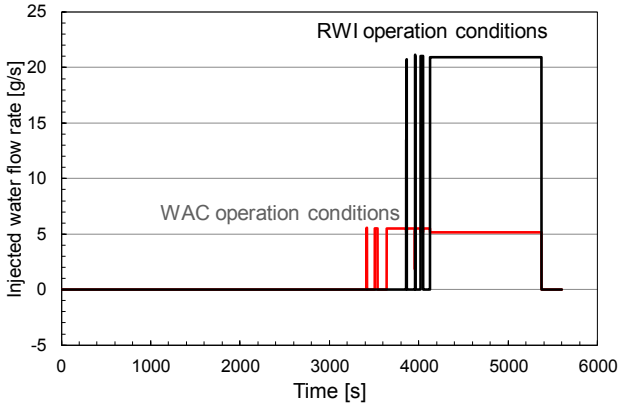

Figure 5. Simulation conditions of injection water flow rates for WAC and RWI [6]

The ignition rotational speed of the prototype microturbine system was 5,000 rpm. Discharge pressure of the compressor was not high enough to secure a distinguishable pressure increase in the map of the compressor characteristic curves. The initial rotational speed was set to 10,000 rpm. The fuel was supplied to only the pilot burner from the start to the rotational speed of 40,000 rpm. At 40,000 rpm, fuel was also supplied to the main burner. From this rotational speed and higher, fuel flow rate was increased. Fuel flow rate of the main burner that was supplied was much more than the planned amount of the fuel supply rate to prevent misfiring because the temperature of air sent from the recuperator was not warm enough to keep the stable combustion condition during warming-up of the recuperator. When the effect of the recuperator begun to appear, the fuel flow rate was reduced gradually to reach the planned amount of the fuel flow rate. A similar fuel supply procedure has also been used in another recuperated gas turbine [2].

Injection water was given at the timing shown in Fig. 5. It was supplied first for WAC, which was done as two pulse injections for a trial, and then it was continuously supplied after the trial. During the continuous supply period for WAC, three trial pulse injections for RWI were carried out to check stability of the turbine system operation. Continuous supply for RWI was done after that. The maximum amount of supplied water was about 2.5% of the rated air flow rate of the compressor: 0.5% was for WAC operation, 2.0% was for RWI operation. The initial diameter of a droplet was given as 20 μm.

The atmospheric conditions were temperature of 30 °C, pressure of 100 kPa, and relative humidity of 70%. Temperature of the injected water was 15 °C. The dynamic simulation was started by giving the operation conditions of rotational speed, fuel flow rate, and injection water for the input data.

4. RESULTS AND DISCUSSION

4.1 Running Curve

The running curve results were plotted in the characteristic map of the compressor shown in Fig. 3 and Fig. 6 is an enlarged chart of the characteristic map around the rated rotational speed. The solid thick line shows simulation results, and the small circles are measured results [6]: red circles mean measured results without WAC and RWI, blue circles mean measured results with WAC only and green circles mean measured results with WAC and RWI. The simulation results show good agreement with the measured results in the operation region for increasing rotational speed where β was decided to fit the measured results as a function of only the rotational speed shown in Eq. (5).

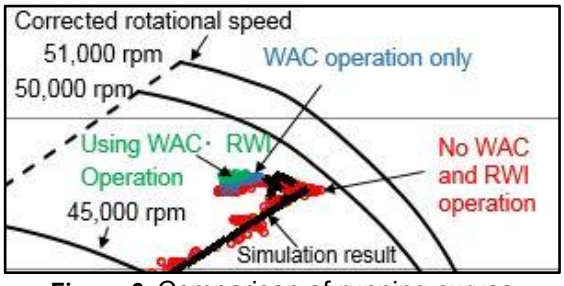

Figure 6. Comparison of running curves

The rotational speed from 49,990 to 50,490 rpm, which corresponds to the corrected rotational speed in Fig. 6 from 48,400 to 49,000 rpm, was considered as the rated rotational speed region and β was modeled by the function of the generator output power. Measured results of the corrected mass flow rate in the range of rotational speeds from 49,990 to 50,490 rpm vary from 1.06 to 1.20 kg/s. On the other hand, the simulation results show a narrow band for the corrected mass flow rate change. This discrepancy might be caused by insufficient modeling for β in that rotational speed region.

4.2 Pressure and Temperature

Figure 7 compares simulation and measured results [6] for the discharge pressure of the compressor. Though simulation results are a little higher than the measured results in the region from 1,000 to 3,200 s, they generally show good correspondence with the measured results from the starting region to the rated rotational speed region.

Once the rotational speed was decreased after 3,200 s had passed, trial injections of WAC were begun after 3,400 s. For the two trial injections of WAC, small jumps of the pressure are recognized both for simulation and measured results. The operation matching point of the compressor moves to the high pressure region in the map of the characteristic curves because the corrected rotational speed shifts to the high speed region due to the air temperature drop effect by WAC in the compressor inlet; however, it is difficult to recognize these rotational speed shifts in Fig. 6 because the rotational speed change is very small. Figure 8 shows the measured corrected rotational speed history. Analogous to the compressor outlet pressure shown in Fig. 7, the increase in the corrected rotational speed brought about by WAC operation also can be recognized specifically in Fig. 8. The pressure jumps due to the shift of the matching point by WAC can be captured in this simulation.

Simulation results of gas temperature of the combustor and the turbine inlet are compared with those of the measured results in Fig. 9. In the region from 600 to 3,000 s, they show large discrepancies. Fuel of the main burner began to be supplied at about 600 s. Combustion of the main burner tends to be unstable just after the fuel was supplied to it because the temperature of air sent from the recuperator did not rise sufficiently.

Figure 10 shows the measured combustion efficiency which is used in the calculation of Eq. (8). For the region from 600 to 1,500 s, which corresponds to beginning the main fuel supply, the measured combustion efficiency fluctuated until stable combustion was obtained. The measured combustion efficiency may have included a quite large measurement error due to the unstable and incomplete combustion. This combustion efficiency fluctuation in the region from 600 to 1,500 s directly affects gas temperature changes of the turbine inlet.

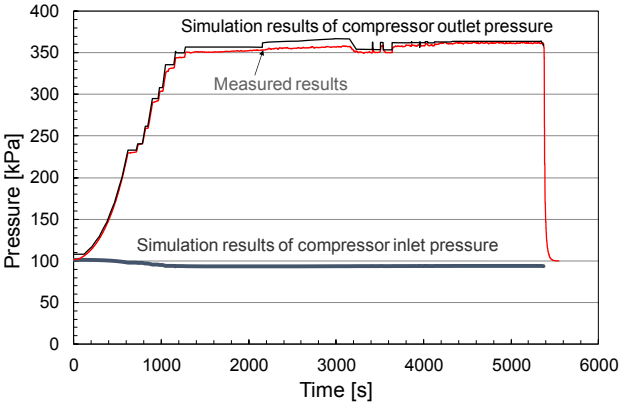

Figure 7. Pressure histories of compressor

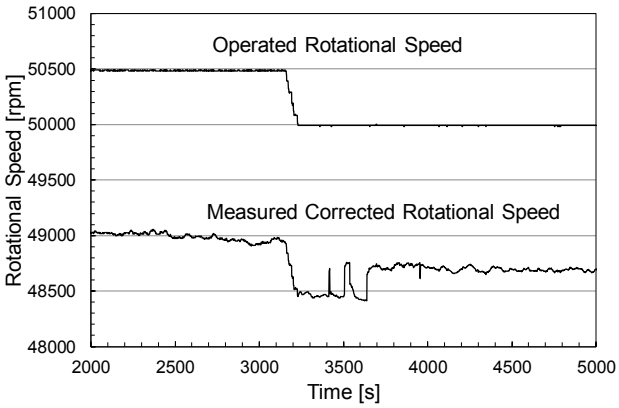

Figure 8. Measured corrected rotational speed

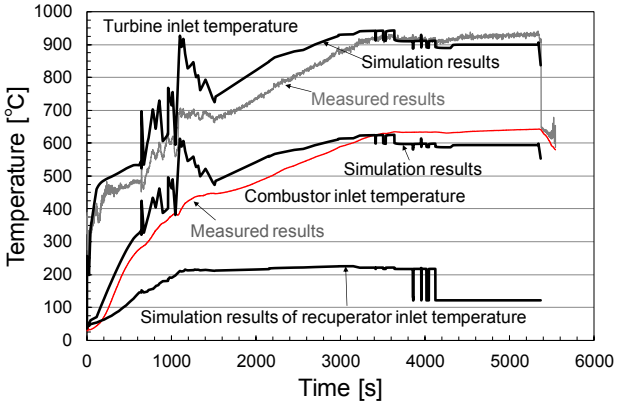

Figure 9. Temperature histories

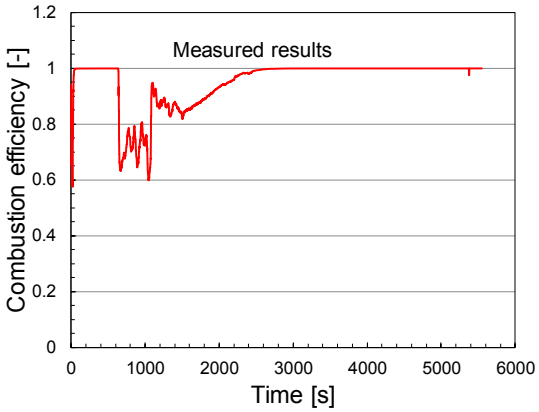

Figure 10. Measured combustion efficiency

Furthermore, the recuperator effectiveness of the simulation model reaches the design value of the specification at 1,300 s while the actual value seems to be lower than that. The recuperator of the prototype turbine system has a quite large heat capacity which was judged to be about 240 kJ/K because the total weight of the recuperator was about 480 kg. The region which shows a large discrepancy between the simulation results and the measured results is the period of the recuperator warming.

Combustor inlet temperature is also affected by these spikes of the measured combustion efficiency due to the effect of the heat transfer from the combustor to the compressor. So, both spikes of turbine inlet temperature and combustor inlet temperature correspond respectively.

Simulation results of the air temperature at the recuperator inlet are also shown in Fig. 9. A clear temperature drop at the recuperator inlet can be seen due to the RWI effect.

4.3 Compressor Driving Power, Turbine Output, and Generator Output Power

Simulation results of the turbine output power, the compressor driving power, and the generator output power are compared with those of the measured results [6] in Fig. 11. In the right-side enlarged chart, the power histories are expanded in the region of WAC and RWI operations. Generator power jumps which occurred at the timing of WAC and RWI operations can be captured in the simulation results. Slight drops of the compressor driving power also appear at WAC operations. Property change of the flue gas is small because the flow rate of the injected water is about 2.0 %. The change of the turbine work can be brought about by the inlet condition change of the pressure and heat recovery from the exhaust gas. This simulator was judged to be applicable in the realization of microturbine system behavior applying both WAC and RWI.

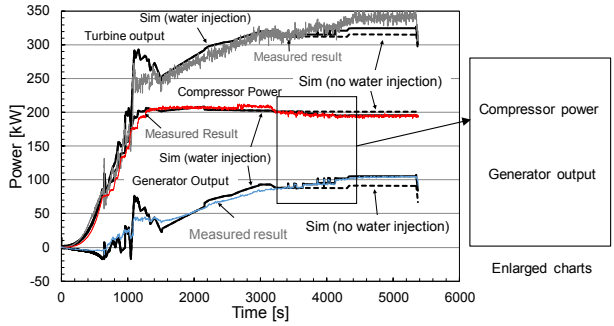

Figure 11. Power histories and effects of WAC and RWI

4.4 Influence of Heat Penetration into the Compressor

As mentioned before, heat penetration from the turbine to the compressor is considered in the simulator. It is difficult to make an accurate heat transfer simulation model using a simple model because the structure of that section is quite complicated. A simple model of the heat transfer is applied in this simulator. It is assumed that temperature rise in the compressor will occur, based on heat transfer in proportion to the temperature difference between the turbine inlet and the compressor outlet. The proportionality constant is set as 0.04 for the simulations.

In Fig. 12, simulation results without heat penetration are shown by broken lines while the solid lines are the same as the simulation results shown by the solid lines in Fig. 11. Just after reaching the rated rotational speed which is at about 1,200 s, a big difference appears between the results with the heat penetration and those without the heat penetration for the compressor driving power and the generator output power. This suggests that heat penetration into the compressor for a microturbine has a large effect on turbine performance.

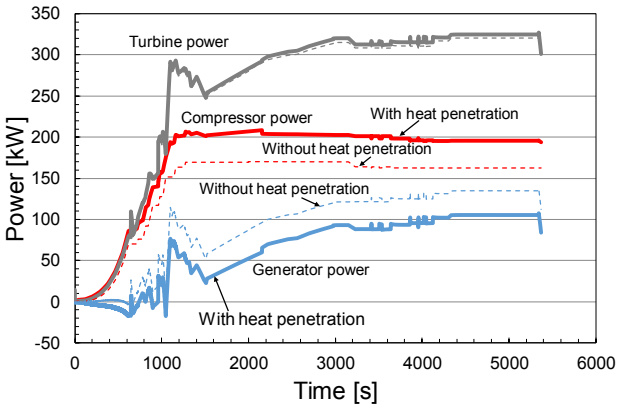

Figure 12. Effect of heat penetration into the compressor on performance

4.5 Influence of WAC and RWI on Generator Output Power

Fig. 13 shows breakdowns of the power augmentation which are effects of WAC and RWI. As effects of WAC operation, the compressor power drop is calculated as about 4 kW due to the wet compression effect. Both the driving power of the compressor and the turbine output power increase because of the shift of the operation matching point. The turbine output power increase of 4 kW is obtained in the simulation. Total driving power decrease of the compressor becomes 3 kW which is the summation of the increased power of 1 kW and the decreased power of -4 kW. Generation output power augmentation of about 7 kW by WAC operation is finally obtained in the simulation.

As effects of RWI operation, increase of the turbine power and decrease of the compressor power in the simulation results are also observed. Generation output power augmentation of about 8 kW by RWI operation is obtained. Increase of the turbine power by RWI is mostly introduced by the increase of the heat recovery from the exhaust gas of the turbine. As RWI is implemented for the downstream region of the compressor, RWI is thought to give no effect on the driving power reduction of the compressor. However, a slight decrease of the compressor power is observed in both measured and simulation results. The heat penetration into the compressor seems to decrease because the turbine inlet temperature decreases when RWI is operated. This heat penetration reduction affects

the reduction of compressor driving power. The compressor power decrease of 2 kW and the turbine output power increase of 6 kW by RWI are obtained.

The total generator output power augmentation of about 15 kW is obtained, compared to the value just before the WAC operation. These power augmentations show relatively good agreement with the measured values for the prototype microturbine operation test [6], which were the power increase of 6.5 kW by WAC, 10.5 kW by RWI, and 17 kW by both WAC and RWI operations. In Fig. 13, the discrepancy of the power augmentation between the measured and simulation results of RWI is higher than that of WAC. There are thought to be two reasons for this. One is that the fluctuation of the measured turbine power in RWI operation is more than that of WAC operation. Measurement errors in RWI operation seem to be larger than those of WAC operation. The other is the influence of coarse droplets which are generated by the collision of fine droplets in the water injection duct. All these coarse droplets cannot evaporate in the duct and some enter the recuperator. Evaporation of the coarse droplets in the recuperator seems to induce an increase in the recuperator effectiveness. Advanced models for the droplet evaporation, which can handle the effect of coarse droplets generated by the droplet collision that occurs in the limited space of the duct, are expected to improve the simulation accuracy in the next step of the study. In the total output power augmentation of the generator by WAC and RWI operations, about 1/3 is brought about by the reduction of the compressor driving power and the remaining 2/3 is brought about by the increase of the turbine output power.

Injected droplets for WAC and RWI are not completely evaporated in the simulation. As no drain was observed in the prototype microturbine operation test, the residual water from the injected water amount is assumed to evaporate completely in the downstream region of the compressor for WAC and in the recuperator for RWI. As mentioned in Section 2.7 about the simulation models for WAC and RWI, mass and enthalpy of the residual water are added to the wet air. Though the mass flow rate increase by injected water also contributes to the power augmentation, the amount of mass increase rate is only 0.5 – 2.5% of the mass of air flow. So, the contribution of power augmentation by the mass increase which is included in the increase of the turbine output power was thought to be limited in the range of 0.4 – 2 kW in the prototype microturbine operation test.

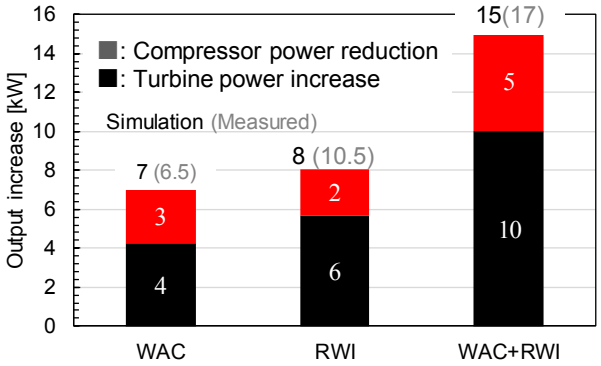

Figure 13. Effects of WAC and RWI

CONCLUSIONS

A dynamic simulator for a microturbine which applies WAC and RWI was developed to clarify their quantitative contributions to power augmentation. Simulation and measured results of the prototype microturbine operation test were compared and the following conclusions were obtained.

(1) By incorporating simple simulation models of water droplet evaporation in the simulator, effects of WAC and RWI could be calculated. These effects were verified with the augmentation of the generator output power. Simulation results showed quite good agreement with the measured results. This simulator was judged to be applicable in the realization of microturbine system behavior applying both WAC and RWI.

(2) In the total output power augmentation of the generator by WAC and RWI operations, about 1/3 was brought about by the reduction of the compressor driving power and about 2/3 was brought about the increase of the turbine output power.

(3) When the heat penetration from the turbine to the compressor was considered, the simulation results showed good agreement with the measured results when a simple model of the heat transfer, which is based on heat transfer in proportion to the temperature difference between the turbine inlet and the compressor outlet, was applied in the simulator.

ACKNOWLEDGEMENTS

Development of the simulator has been conducted jointly between Tohoku University and Tohoku Electric Power Co., Inc. The authors express their gratitude to Tohoku Electric Power Co., Inc. for its support.

REFERENCES

[1] S. Gamou, K. Ito, and R. Yokoyama. Optimal operational planning of cogeneration systems with microturbine and desiccant air conditioning units. *Journal of Engineering for Gas Turbines and Power*, 127(3):606-614, 2005.

[2] S. Higuchi, et al. Test results from the advanced humid air turbine system pilot plant – Part 1:

Overall performance. *ASME Conference Proceedings*, ASME Paper No.GT2008-51072, 2008.

[3] T. Williamson, M. Luker and R. L. Hack. Microturbine performance improvement through the implementation of inlet air cooling". *ASME Conference Proceedings*, ASME Paper No. GT2005-68377, 2005.

[4] J. Parente, A. Traverso and A. F. Massardo. Micro humid air cycle, Part A: Thermodynamic and technical aspect. *ASME Conference Proceedings*, ASME Paper No. GT-2003-38326, 2003.

[5] W. De Paepe, M. Carrero, S. Bram and F. Contino. T100 micro gas turbine converted to full humid air operation – A thermodynamic performance analysis. *ASME Conference Proceedings*, ASME Paper No. GT2015-43267, 2015.

[6] S. Nakano, T. Kishibe, H. Araki, M. Yagi, K. Tsubouchi, M. Ichinose, Y. Hayasaka, M. Sasaki, T. Inoue, K. Yamaguchi and H. Shiraiwa. Development of a 150 kW microturbine system which applies the humid air turbine cycle. *ASME Conference Proceedings*, ASME Paper No. GT2007-28192, 2007.

[7] S. Nakano, T. Kishibe, T. Inoue, and H. Shiraiwa. An advanced microturbine system with water-lubricated bearing. *International Journal of Rotating Machinery*, Volume 2009, 718107, 2009.

[8] S. M. Camporeale, B. Fortunato, M. Mastrovito. A modular code for real time dynamic simulation of gas turbines in Simulink. *Journal of Engineering for Gas Turbines and Power*, 128:506-517, 2006.

[9] R. A. Roberts and S. M. Eastbourn. Modeling techniques for a computational efficient dynamic turbofan engine model. *International Journal of Aerospace Engineering*, 2014, Article ID 283479, 2014.

[10] H. Perez-Blanco and T. B. Henricks. A gas turbine dynamic model for simulation and control. *Proceedings of International Gas Turbine & Aeroengine Congress & Exhibition*, Paper No. 98-GT-78, 1998.

[11] H. Schlichting. *Boundary Layer Theory*, McGraw-Hill, New York, 1968.

[12] A. J. White and A. J. Meacock. An evaluation of the effects of water injection on compressor performance. *ASME Conference Proceedings*, ASME Paper No. GT-2003-38327, 2003.

[13] A. H. Lefebvre. *Gas Turbine Combustion*. Taylor & Francis, Bristol, 1983.

[14] K. Seki, S. Nakano and Y. Takeda. Dynamic simulations of microturbines. *Proceedings of International Gas Turbine Congress*, IGTC2015-TuAMD.3, 2015.

[15] O. E. Balje. *"Turbomachines: A Guide to Design, Selection and Theory*. John Wiley & Sons, New York, 1981.

[16] J. M. Owen and R. H. Rogers. *Flow and Heat Transfer in Rotating – Disc Systems Volume 1 – Rotor-Stator Systems*, John Wiley & Sons, New York, 1989.

[17] C. Myoren, Y. Takahashi, M. Yagi, T. Shibata and T. Kishibe. Evaluation of axial compressor characteristics under overspray condition. *ASME Conference Proceedings*, ASME Paper No. GT2013-95402, 2013.

[18] F. P. Incropera and D. P. Dewitt. *Fundamentals of Heat and Mass Transfer*, John Wiley and Sons, New York, 1985.

[19] S. K. Aggarwal and F. Peng. A review of droplet dynamics and vaporization modeling for engineering calculations. *Journal of Engineering for Gas Turbines and Power*, 117:453-461, 1995.

[20] M. Kimura, H. Koharagi, K. Imaie, S. Dodo, H. Arita and K. Tsubouchi. A permanent magnet synchronous generator with variable speed input for co-generation system. *Proceedings of Power Engineering Society Winter Meeting*, *IEEE*, 7023560, 2001.